RESEARCH ARTICLE

ADVANCED HEALTHCARE MATERIALS
www.advhealthmat.de

Pincer-Type Pt(II)-NHC Antibody-Drug Conjugate for HER-2-Targeted Chemoimmunotherapy

Tao Huang, Wan-Qiong Huang, Gui-Feng Huang, Xiao-Long Wei, Yong-Liang Huang, Tao Liu, Yungen Liu, Wen-Xiu Ni,* and Chi-Ming Che**

Platinum-based chemotherapy drugs play an indispensable role in clinical cancer treatment, but exhibit considerable side effects due to their non-specific mechanism of killing cancer cells and normal cells. In this regard, the use of antibodies conjugated to anti-cancer platinum complexes will enable better differentiation of cancer cells from normal cells. Here, six pincer-platinum(II) NHC (N-heterocyclic carbene) complexes are reported, one of which has an amino group on the N-alkyl group of the NHC ligand. This platinum(II) complex is used as the payload for platinum(II)-based antibody-drug conjugate (ADC) targeting human epidermal growth factor receptor 2 (HER-2). Notably, this ADC can specifically bind to the HER-2 antigen, distinguish target cells from non-target cells, and exhibit good anti-tumor activity in vitro and in vivo.

T. Huang, G.-F. Huang, Y.-L. Huang, T. Liu, W.-X. Ni
Department of Medicinal Chemistry
Shantou University Medical College
Shantou, Guangdong 515041, P. R. China
E-mail: wxni@stu.edu.cn

T. Huang, G.-F. Huang, T. Liu, W.-X. Ni
Chemistry and Chemical Engineering Guangdong Laboratory
Shantou, Guangdong 515021, P. R. China

W.-Q. Huang, X.-L. Wei
Department of Pathology
Cancer Hospital of Shantou University Medical College
Shantou, Guangdong 515041, P. R. China

Y. Liu
Department of Chemistry
Southern University of Science and Technology
Shenzhen, Guangdong 518055, P. R. China
E-mail: liuyg@sustech.edu.cn

C.-M. Che
State Key Laboratory of Synthetic Chemistry and Department of Chemistry
The University of Hong Kong
Hong Kong, P. R. China
E-mail: cmche@hku.hk

C.-M. Che
Laboratory for Synthetic Chemistry and Chemical Biology Limited
Hong Kong Science and Technology Parks
Units 1503–1511, 15/F, Building 17W, New Territories, Hong Kong, P. R. China

The ORCID identification number(s) for the author(s) of this article can be found under https://doi.org/10.1002/adhm.202403449

DOI: 10.1002/adhm.202403449

1. Introduction

After the Food and Drug Administration (FDA) approved cisplatin for anti-cancer treatment in 1978, platinum-based chemotherapy drugs began to play an indispensable role in clinical chemotherapy regimens.[1] Known as cisplatin, it primarily damages DNA (deoxyribonucleic acid) leading to apoptotic cell death, and is associated with side effects such as nephrotoxicity, ototoxicity, neurotoxicity, and bone marrow suppression.[2] In recent years, some new pincer platinum(II) complexes have shown micromolar level cytotoxicity to a variety of cancer cells, such as the ones with N-heterocyclic carbene ligand, which mainly bind to non-DNA biomolecules.[3] Necroptosis is a regulated form of necrosis that is independent of caspases but highly dependent on biomolecules, including receptor-interacting protein kinase 1 (RIPK-1) and 3 (RIPK-3). Mixed lineage kinase domain-like (MLKL) was originally thought to be a non-apoptotic form of cell death that can circumvent chemotherapeutic drug-induced apoptosis resistance.[4] There are few reports on necroptosis induced by chemotherapy drugs, especially metal-based chemotherapy drugs.[5] Studies have shown that necroptosis is associated with the generation of immunogenic activities, including intracellular ROS (reactive oxygen species) levels and ER (endoplasmic reticulum) stress-mediated immunogenic cell death (ICD).[4b,6] In recent years, platinum complexes have been found to act as ICD inducers and stimulate effective anti-cancer immune responses.[7] These ICD inducers have shown great potential in the field of anticancer therapy.[8] Among them, oxaliplatin is a representative metal compound with type I ICD inducer effect.[9] Importantly, an increasing number of platinum complexes have been reported to possess ICD-inducing properties.[7b,d,10] Most ICD inducers trigger endoplasmic reticulum stress and the production of reactive oxygen species (ROS). Although some anti-cancer platinum complexes with different mechanisms of action besides targeting DNA have been developed, there are still problems of indiscriminate killing of cells (normal cells and cancer cells) and side effects.[11] Therefore, it is crucial to develop new anti-cancer platinum compounds that are more effective and have higher target selectivity.[12] Since 2000, the first ADC (antibody-drug conjugate) Mylotarg (gemtuzumab ozogamicin) has been approved by the FDA for the treatment of acute myeloid leukemia.[13] Antibodies, linkers, and cytotoxic molecules together form antibody-drug conjugates with targeting capabilities.[14] Due to the

specificity of antibodies, some cytotoxic molecules with high toxicity and narrow therapeutic window are used in ADCs, such as MMAE (Monomethyl auristatin E) and MMAF (Monomethyl auristatin F) derivatives.[15] Nonetheless, in the past 20 years, there have been only sporadic reports on the application of anti-cancer platinum complexes in ADCs.[16] In addition, due to the low admission velocity and content level of ADC entering cancer cells, it is difficult to achieve therapeutic effect using cisplatin-based chemotherapy drugs as the payload of ADC in some cases.[17] The use of platinum-based complex antibodies can improve the accumulation of complexes in tumor and reduce their side effects.[18] In the development of ADCs, small organic molecules with high cytotoxicity (e.g., DM1, Dxd, and clinically used chemotherapeutic compounds) with low nano-molar or even pico-molar toxicity are often used as payloads. These clinically used cytotoxic payloads (mainly organic compounds) often have non-specific molecular targets such as DNA and tubulin. In fact, current chemotherapies are often unable to kill cancer stem cells and eliminate metastatic cancer cells at doses used clinically. On the other hand, they exhibit adverse and sometimes severe side effects due to their high toxicity and non-specific mechanism of action. There is ample evidence that current ADCs suffer from off-target toxicities caused by the cytotoxicity of the payload. The more toxic and less specific the payload is, the more significant the toxic side effects it will produce. We take a novel approach ADC development using payloads targeting key oncogenic proteins for which effective inhibitors are still lacking in the clinic. Although these payloads may be less cytotoxic than the highly cytotoxic chemotherapies used clinically. their more specific anti-cancer mechanisms of action may help reduce toxicity caused by off-target side effects. In this effort, we are interested in developing ADCs using cytotoxic metal complexes with specific anti-cancer mechanisms of action as payloads. Over the past few years, we have extensively developed and investigated pincer d8 metal complexes as potent anti-cancer drug candidates. These pincer d8 metal complexes, exemplified by the Pt-NHC complex described in this study, are stable under cellular conditions and can form stable ADCs. Although the toxicity of the Pt(II)-NHC complex is only at the micro-molar level, it can effectively target to multiple oncogenic proteins,[3f,19] trigger tumor cell necroptosis, and synergistically induce immunogenic cell death (ICD). Our previous study[3g] showed that the pincer Pt-NHC complex exhibited potent anti-tumor effects and safety in vivo. By synergistically combining the specific targeting effect of anti-bodies on specific types of cancer cells and the oncogenic protein targeting effect of Pt-NHC complexes, we hope to develop more effective and safer ADCs for cancer treatment. Herein, novel highly efficient antitumor platinum(II) complexes with [C^N^N] and *N*-heterocyclic carbene ligands were synthesized and conjugated to trastuzumab. The resulting platinum(II)-based antibody-drug conjugate targeting HER-2 is designed to provide an efficient platform for tumor-specific delivery.

2. Results and Discussion

2.1. Synthesis and Characterization of Platinum(II) Complexes

The PF_6^- salt structures of pincer Pt(II) complexes (**Pt-1** to **Pt-6**) are shown in **Figure 1**. These complexes were synthesized by

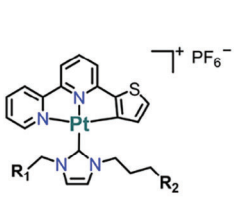

	R_1	R_2
Pt-1		
Pt-2	$-CH_3$	-OH
Pt-3	$-(CH_2)_2CH_3$	-OH
Pt-4	$-(CH_2)_4CH_3$	-OH
Pt-5	-Ph	-OH
Pt-6	-Ph	$-PO(OCH_2CH_3)_2$

Figure 1. Chemical structures of platinum(II) complexes.

Table 1. The IC_{50} value of C^N^N tridentate NHC platinum(II) complexes and cisplatin on cells (μM, 72h).

Cell line	MCF-7	MDA-MB-231	BT-474	SK-BR-3	SK-OV-3
Pt-1	5.8 ± 1.1	8.0 ± 1.7	6.0 ± 0.8	3.8 ± 0.2	9.7 ± 0.4
Pt-2	2.8 ± 0.3	22.9 ± 2.3	2.0 ± 0.4	1.6 ± 0.2	23.5 ± 2.2
Pt-3	1.2 ± 0.4	5.1 ± 0.8	0.66 ± 0.15	0.42 ± 0.04	4.9 ± 0.6
Pt-4	0.60 ± 0.02	2.9 ± 0.5	0.54 ± 0.18	0.30 ± 0.02	1.3 ± 0.2
Pt-5	1.5 ± 0.2	6.7 ± 0.9	1.0 ± 0.2	1.0 ± 0.1	3.7 ± 0.2
Pt-6	7.9 ± 0.7	16.0 ± 1.6	3.7 ± 0.4	5.8 ± 1.1	27.1 ± 4.1
cisplatin	1.9 ± 0.1	17.6 ± 1.9	20.6 ± 0.6	2.4 ± 0.1	3.6 ± 0.1

refluxing cyclometalated Pt(II) precursor ([Pt(C^N^N)Cl]) and imidazolium salt in acetonitrile under alkaline conditions, and obtained as yellow or orange solids according to reported methods (Schemes S1 and S2, Supporting Information).[3g] Detailed synthetic procedures and characterization data for intermediates and final compounds are included in the Supporting Information. The X-ray crystal structures of **Pt-2** to **Pt-6** (Figure S1, Supporting Information) have been determined, showing that Pt atoms adopt a twisted planar molecular geometry and are coordinated by one C atom and two N atoms of [C^N^N] ligand and the C atom of the imidazole carbene ligand. As shown in Tables S1 and S2 (Supporting Information), the Pt–C and Pt–N distances (1.956 (5)–2.125 (13) Å) are within the normal range. Photophysical data for **Pt-1** to **Pt-6** were collected at room temperature and summarized in Figure S2 and Table S3 (Supporting Information). These platinum complexes are luminescent in degassed CH_2Cl_2 with emission λ_{max} at 606–611 nm and 641–647 nm, emission lifetime (τ) of 1.93–2.50 μs, and emission quantum yield (Φ) of 0.039–0.061. The stability of **Pt-1** to **Pt-6** was evaluated by ultraviolet-visible spectroscopy (UV–vis) in various solutions at 25 °C. All complexes remained stable during the 24-h assay in neat DMSO or PBS solutions (with 1% DMSO, PBS = phosphate-buffered saline, pH 7.4, Figures S3 and S4, Supporting Information).

2.2. Cytotoxicity, Necroptosis, and Immunogenic Cell Death

We tested the in vitro anti-cancer effect of $[(C^N^N)Pt^{II}(NHC)]^+$ complex on 5 different cancer cell lines, MDA-MB-231, MCF-7, BT474, SK-BR-3 and SK-OV-3, using Naphthol Blue Black (NBB) method. As shown in **Table 1**, their cytotoxicity and IC_{50} (half maximal inhibitory concentration) values range from 0.30 to 27.1 μM. The anti-proliferative activity of the $[(C^N^N)Pt^{II}(NHC)]^+$ complex appears to be related to the length of the carbene *N*-alkyl carbon side chain. This is because the longer the alkyl carbon

chain, the greater the lipid solubility and the easier it is to enter cells.

As shown in Figure S2 (Supporting Information), **Pt-1** displays emission at wavelength 606 nm suitable for cell imaging. When SK-OV-3 cells were incubated with **Pt-1** for 6 h, red emission was observed upon excitation at 405 nm (**Figure 2a**; Figure S5, Supporting Information). Subsequent examination of subcellular colocalization using mitochondria-specific Tracker Green showed high concordance, with a Pearson Correlation Coefficient (PCC) was 0.78. The results show that **Pt-1** mainly accumulates in mitochondria and may cause mitochondrial damage. Mitochondrial membrane potential (ΔΨm), which is closely linked to mitochondrial function, was observed using JC-1 staining. As shown in Figure S6 (Supporting Information), compared with the "control" group, **Pt-1**-treated cells showed a significant increase in green fluorescence and a decrease in red fluorescence, manifested by a decrease in ΔΨm. Mitochondria produce cellular energy in the form of adenosine triphosphate (ATP) to support various cellular activities,[20] so we studied ATP production after **Pt-1** treatment. As shown in Figure 2b, in the presence of different concentrations of **Pt-1**, intracellular ATP levels were significantly reduced, showing that **Pt-1** has a significant impact on cellular energy production.

It is well known that reactive oxygen species (ROS) play a critical role in redox homeostasis. The main sites of cellular ROS generation include mitochondria and endoplasmic reticulum.[21] To evaluate the effect of **Pt-1** on ROS generation, the intracellular fluorescence level was determined by flow cytometry and microscopy imaging using 2′,7′-Dichlorodihydrofluorescein diacetate (DCFH-DA) assay. As described in the literature, DCFH-DA is widely used to detect intracellular ROS.[22] When the acetate group is removed by intracellular esterases and then oxidized by intracellular ROS, the non-fluorescent DCFH-DA is converted into a charged form of the dye, 2′,7′-dichlorofluorescein (DCF), which exhibits high fluorescence. In addition, DCF is not easily released from cells, so it can accumulate inside cells and detect ROS.[23] A significant increase in fluorescence intensity was observed in SK-OV-3 cells treated with **Pt-1** for 6 h (Figure 2c). Analysis of ROS expression after 6-h of **Pt-1** treatment using fluorescence microscopy revealed a significant increase in ROS levels (Figure S7, Supporting Information). Since endoplasmic reticulum (ER) stress is a potential downstream effect of ROS production,[21] we measured glucose regulatory protein 78 (GRP78),[24] phosphorylated eukaryotic initiation factor 2a (p-eIF2a),[7a] and C/EBP homologous protein (CHOP). Through Western blot (WB) analysis, increased expression of GRP78, p-eIF2a, and CHOP was observed in SK-OV-3 cells (Figure 2d), indicating that ER stress occurred during **Pt-1** treatment.

To elucidate the mechanism of **Pt-1**-induced cell death, caspase-mediated apoptosis proteins were first detected by Western blot analysis (Figure S8, Supporting Information). Treatment with high concentrations of **Pt-1** treatment resulted in a decrease in caspase 8 and an increase in cleaved caspase 3, indicating the presence of apoptotic signals. Impaired caspase 8 activity has been previously reported to lead to necroptosis.[25] In addition, the addition of caspase-mediated apoptosis (Z-VAD-FMK) and necroptosis (necrostatin-1) inhibitors changed the ability of **Pt-1** to kill SK-OV-3 cells, indicating that **Pt-1** may also induce necroptosis (Figure S9, Supporting Information). Necroptosis is a form of regulated cell death characterized by the kinase activity of receptor-interacting protein kinase-1 (RIPK1), RIPK3, and their substrate mixed lineage kinase domain-like (MLKL).[26] Therefore, the levels of RIPK1, RIPK3, and MLKL, and their phosphorylation expression, as hallmarks of necroptosis, were determined by Western blot analysis. As shown in Figure 2e, after incubation with **Pt-1**, the expressions of P-RIPK1, P-RIPK3, and P-MLKL were upregulated in a dose-dependent manner, showing that **Pt-1** effectively triggers necroptosis in SK-OV-3 cells.

Given that necroptosis is associated with activation of antitumor immunity, coupled with findings of elevated intracellular ROS levels and ER stress, we explored the potential of **Pt-1** to induce immunogenic cell death (ICD). ICD is characterized by the release of damage-associated molecular patterns (DAMPs), including relocalization of the ER-resident chaperone protein calreticulin (CRT) to the plasma membrane, extracellular secretion of ATP, and extracellular release of nucleocytoplasmic high mobility group box 1 (HMGB1) protein from dying cells.[7a,b,27] Therefore, these biochemical hallmarks were examined in **Pt-1**-treated SK-OV-3 cells. Confocal microscopy was used to detect changes in the fluorescence intensity of CRT and HMGB1 through immunostaining. An increase in green fluorescence was observed in **Pt-1**-treated SK-OV-3 cells compared with control groups, indicating the presence of enhanced CRT and higher expression level of HMGB1 at the plasma membrane (Figure 2g,h). ATP levels in the supernatants of **Pt-1**-treated SK-OV-3 cells were also evaluated using the Extracellular ATP Assay Kit, and as shown in Figure 2f, **Pt-1** efficiently induced ATP release. Compared with the control group, the ATP level of the 20 μM **Pt-1** group was 1.67-fold, reaching a level comparable to that of the oxaliplatin group. Taken together, these findings indicate that **Pt-1** exhibits excellent mitochondrial accumulation ability to alter energy homeostasis and redox homeostasis by reducing intracellular ATP levels and increasing ROS production, respectively. Sustained elevation of ROS can also trigger catastrophic endoplasmic reticulum stress. Furthermore, additional analysis of cell death revealed that **Pt-1** effectively triggered necroptosis and synergistically initiated ICD, thus enhancing its antitumor efficiency and immune response (Figure 2i). However, despite their extraordinary antitumor potential, their off-target side effects remain unresolved.

2.3. Platinum(II) Complex-Targeted Therapy with Trastuzumab

To improve the tumor selectivity of platinum(II) complex, platinum(II)-based antibody conjugate was synthesized (**Figure 3a**). First, a linker is prepared using valine-citrulline dipeptide as the enzymatic cleavage site and *p*-aminobenzyl group as the spacer linker. Second, **Pt-1** is coupled with linker so that the resulting complex can be connected to the antibody through maleimide (Scheme S3, Supporting Information). When the inter-chain disulfide bonds of trastuzumab are broken, maleimide-bearing **Linker-Pt1** is loaded to specific sites, subsequently producing the platinum(II)-based antibody conjugate **Trastuzumab-Pt1**. Detailed synthesis procedures for intermediates are included in the Supporting Information.

Next, **Trastuzumab-Pt1** was analysed by UV spectrophotometry, SDS-PAGE analysis, and Bicinchoninic Acid assay,

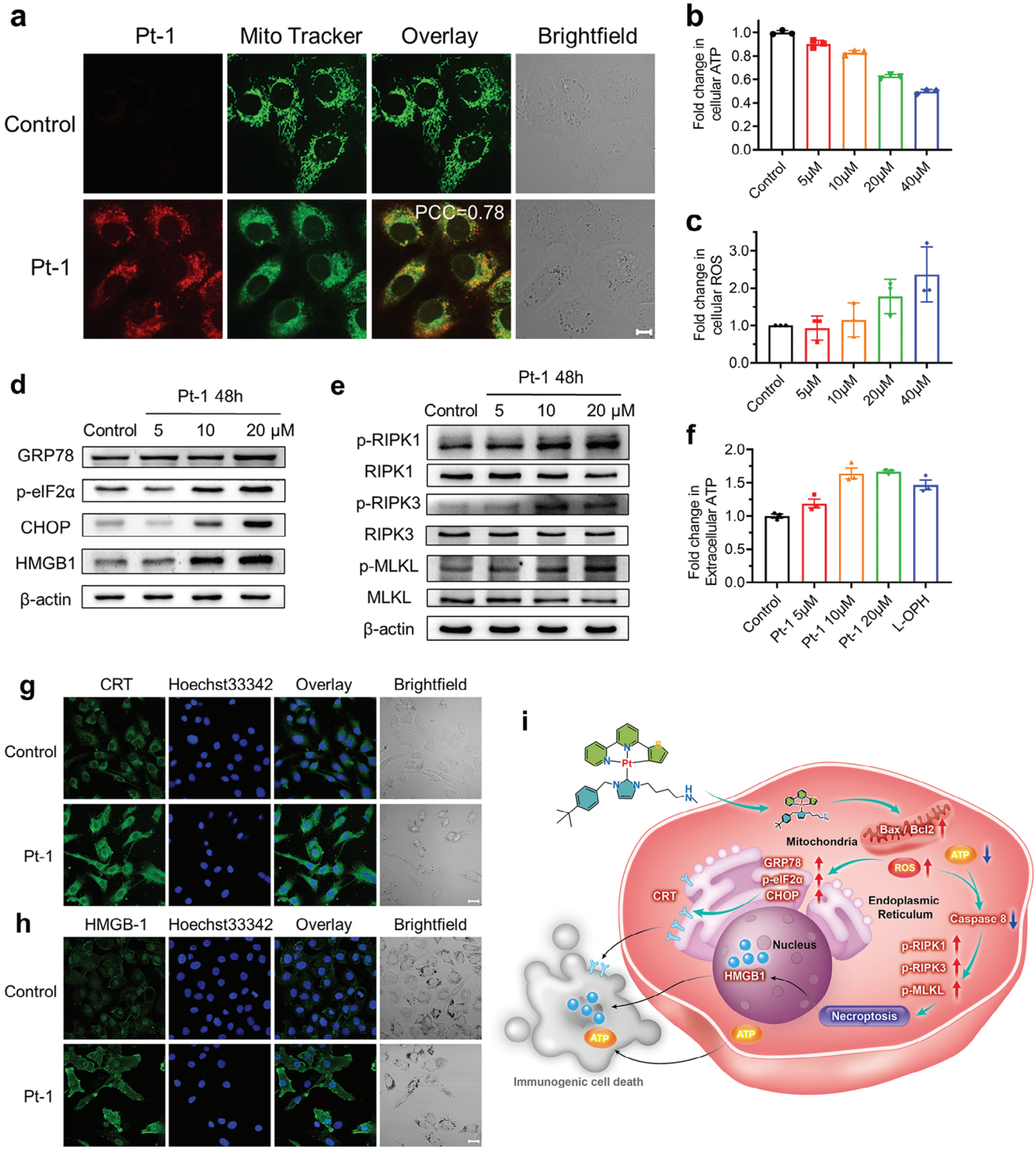

Figure 2. Necroptosis and Immunogenic cell death in cells treated with **Pt-1** complex. a) CLSM (confocal laser scanning microscope) images and analysis of **Pt-1** (6h) with mitotrackers (0.5h) in SK-OV-3 cells. **Pt-1** was excited at 405 nm using an emission range from 550 to 700 nm and mitotrackers were excited at 488 nm using an emission range from 490 to 600 nm (scale bars: 10 μm). b) Fold change of cellular ATP level. c) Fold change of cellular ROS level. d) Expression level of signature protein of endoplasmic reticulum (ER) stress in SK-OV-3 after different treatments via WB. e) Expression level of signature protein of necroptosis pathway in SK-OV-3 after different treatments via WB. f) Fold change of extracellular ATP after **Pt-1** 48 h-treatment by ATP assay kit. g) CLSM images of CRT exposure in SK-OV-3 cells (scale bars: 20 μm). h) CLSM images of HMGB-1 release in SK-OV-3 cells (scale bars: 20 μm). i) Proposed anticancer mechanism of **Pt-1** that induces both mitochondrial damage and endoplasmic reticulum stress, thereby triggering necroptosis and immunogenic cell death.

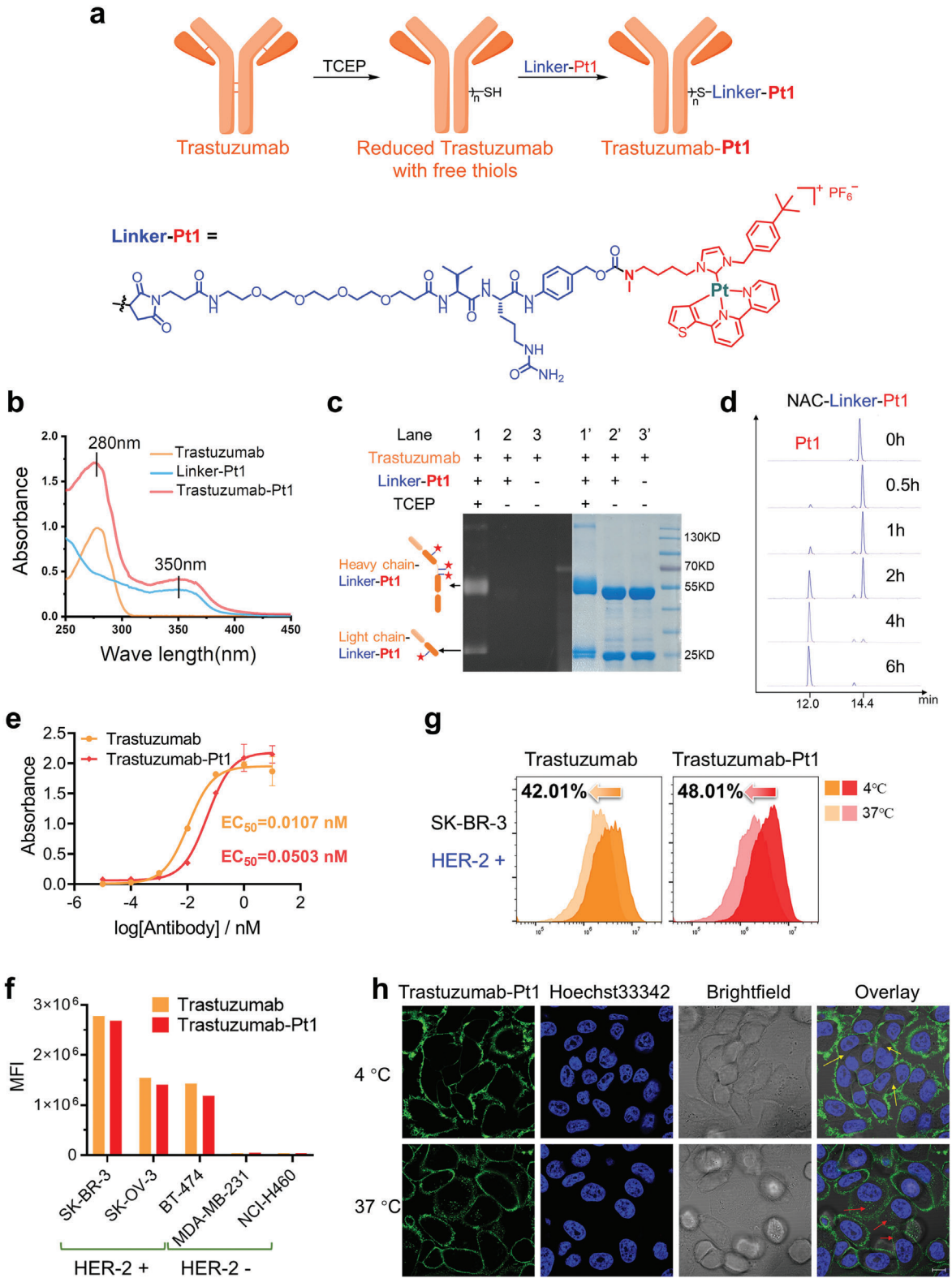

Figure 3. Preparation, characterization, and expected performance of **Trastuzumab-Pt1**. a) The procedure to obtain **Trastuzumab-Pt1**. b) The UV–vis absorbance spectrum of **Trastzuzumab-Pt1**. c) SDS-PAGE analysis of **Trastuzumab-Pt1** under reducing conditions. d) Human cathepsin B-mediated cleavage assay of Linker-Pt1, detected by UPLC-MS. e) The affinity of trastuzumab and **Trastuzumab-Pt1** for HER-2 protein by Indirect-ELISA. f) Flow cytometry-based internalization assay of trastuzumab and **Trastuzumab-Pt1** in SK-BR-3. g) Cell-based binding assay of trastuzumab and **Trastuzumab-Pt1** in different cancer cell lines by flow cytometry. h) CLSM visualization of **Trastuzumab-Pt1** internalization in SK-BR-3 cells (scale bar: 10 μm).

respectively. In Figure 3b, the UV–vis spectrum of **Trastuzumab-Pt1** shows two major peaks at 280 and 350nm, indicating the conjugation of the platinum complex with the antibody. Besides, as shown in Figure 3c, SDS-PAGE (sodium dodecyl sulfate - polyacrylamide gel electrophoresis) analysis showed that the fluorescent bands (heavy chain and light chain of **Trastuzumab-Pt1** after reduction) occurred in lane 1, whereas no detectable fluorescent labels appeared in lane 2 (without TCEP, tris(2-carboxyethyl)phosphine hydrochloride) or lane 3 (only wild-type antibody). After conjugation to **Pt-1**, the bands in lane 1′ were visually shifted up compared to the wild-type antibody as the increase in molecular weight. These results confirm the high selectivity of **Linker-Pt1** for free cysteine residues, and the successful conjugate of platinum complex and the antibody. In addition, **Trastuzumab-Pt1** was almost entirely composed of a single monomeric species (>95% purity) as analyzed by size exclusion chromatography (SEC) (Figure S10, Supporting Information). The coupling efficiency was checked using ultra-high performance liquid chromatography Q Exactive™ Hybrid Quadrupole-Orbitrap™ Mass Spectrometry (Figures S11 and S12, Supporting Information), with an average of 2.6 complexes attached to the antibody (DAR, drug-to-antibody ratio = 2.6).

N-acetylcysteine (NAC) derivatives avoid side reactions caused by free maleimide and mimic antibody amino acid residues.[28] Cathepsin B is a cysteine protease found in the lysosomes of all mammalian cells.[29] Digestion of NAC-Linker-Pt1 with cathepsin-B revealed enzymatic cleavage of the linker at the amide position followed by immolation of *para*-aminobenzyl alcohol, thereby releasing the desired free payload (Figure 3d; Figure S13, Supporting Information). After 6 h of incubation, the **NAC-Linker-Pt1** was completely cleaved and converted to **Pt-1**. This means that **Pt-1** should be successfully released within tumor cells.

At the same time, the targeting of **Trastuzumab-Pt1** was analyzed through Indirect-ELISA and flow cytometry, and the results showed that the conjugate retained binding activity comparable to trastuzumab. **Trastuzumab-Pt1** showed dose-dependent binding activity to HER-2 antigen (Figure 3e), with an EC_{50} (50% effective concentration) value of 0.0503 nM, but its binding affinity was lower compared with trastuzumab (EC_{50} = 0.0107 nM). Flow cytometry was used to detect the HER-2 expression in different human cancer cells, including SK-OV-3, SK-BR-3, BT-474, MDA-MB-231, and NCI-H460.[30] As shown in Figure S14 (Supporting Information), the mean fluorescence intensity (rMFI) ratios of SK-OV-3, SK-BR-3, and BT-474 cells were in the range of 105.1 and 147.2, consistent with HER-2 high-expressing cells. However, MDA-MB-231 and NCI-H460 (rMFI = 1.02–1.14) belong to the HER-2 low expression group. Compared with trastuzumab, **Trastuzumab-Pt1** showed similar binding activity to high HER-2 expressing cells and was able to distinguish cells with different HER-2 expression levels (Figure 3f). In addition, the internalization of **Trastuzumab-Pt1** in target cells was comparable to that of trastuzumab. Since internalization is receptor-mediated endocytosis and energy-dependent, internalization of surface-bound **Trastuzumab-Pt1** or trastuzumab was allowed at 37 °C but not at 4 °C. The extent of internalization of the receptor-antibody complex was calculated as the percent loss of mean fluorescence intensity (MFI) at 37 °C relative to the fluorescent intensity on ice.[31] After 3 h of incubation at 37 °C, flow cytometry confirmed that 48.0%, 42.1% and 25.3% **Trastuzumab-Pt1** entered SK-BR-3, BT-474 and SK-OV-3 cells, respectively (Figure 3g; Figure S15, Supporting Information). Furthermore, immunofluorescence results provided additional evidence that **Trastuzumab-Pt1** was able to enter cells (Figure 3h; Figure S16, Supporting Information). The results showed that although the attached drug/linker slightly affects the binding ability of the antibody, the conjugate still retained antigen recognition.

In vitro cytotoxicity of **Trastuzumab-Pt1** was performed on BT-474, SK-BR-3, SK-OV-3, NCI-H460, MDA-MB-231 cancer cells, and normal breast cells MCF-10A (**Figure** 4a). For HER-2 high-expressing cancer cell lines BT-474, SK-BR-3, and SK-OV-3, cell viability was less than 50% after 96 h of treatment with 5 μM **Trastuzumab-Pt1**. However, the cell viability of the HER-2 low-expression cancer cell lines MDA-MB-231 and NCI-H460 was ≈95% at a concentration of 2.5 μM **Trastuzumab-Pt1** and ≈90% at a concentration of 5 μM **Trastuzumab-Pt1**. At the 5 μM **Trastuzumab-Pt1** dose, the cell viability of MCF-10A was ≈80%. This means that **Trastuzumab-Pt1** can target and destroy cells in high HER-2-expressing cell lines while being almost completely non-cytotoxic against low HER-2-expressing cells and even normal human cells.

Notably, it is worth mentioning that **Trastuzumab-Pt1** is highly specific for high-HER-2-expressing cells in vitro. More importantly, we were able to create 3D tumor cell spheroid models with high and low expression of HER-2. Because the luminescent secondary antibody specifically binds to trastuzumab, significant green emission appears in **Trastuzumab-Pt1**-treated BT-474 tumor spheroids, whereas MDA-MB-231 tumor spheroids show little green emission. This indicates that the conjugate can target 3D tumor spheroids with high HER-2 expression (Figure 4b). To evaluate the ability of **Trastuzumab-Pt1** to target HER-2 high-expressing tumors in vivo, the conjugate was intravenously injected into dual tumor-bearing mice. As shown in Figure 4c, the platinum concentration in SK-OV-3 tumors was significantly higher than in MDA-MB-231 tumors.

In addition, a single tumor-bearing mouse model was established to examine the distribution and active tumor-targeting ability of **Trastuzumab-Pt1**. After being injected intravenously, platinum concentrations in the heart, liver, spleen, lung, kidney, and tumor were assessed by ICP-MS (inductively coupled plasma - mass spectrometry) at 12, 48, and 96h (Figure 4d). The study found that the liver and spleen were the main sites of platinum (12h), with concentrations of 351 and 437 ng g^{-1}, respectively. Notably, tumor platinum concentration increased significantly from 96 to 635 ng g^{-1} at 48 h and remained at a high concentration of 766 ng g^{-1} at 96h.

In addition, platinum concentrations in major tissues such as the heart, liver, spleen, and lung decreased, and the kidneys increased slightly, accompanied by a decrease in blood platinum levels (Figure S17, Supporting Information). Taken together, it may be related to the clearance of **Trastuzumab-Pt1** in the systemic circulation, which means that **Trastuzumab-Pt1** is able to target tumors with high HER-2 expression in vitro and in vivo.

We evaluated the ability of **Trastuzumab-Pt1** to inhibit tumor growth in vivo in mouse xenograft using SK-OV-3 ovarian carcinoma cell-derived tumors. Treatment groups received four doses of 10 or 15mg kg^{-1} intravenously on days 0, 7, 14, and 21.

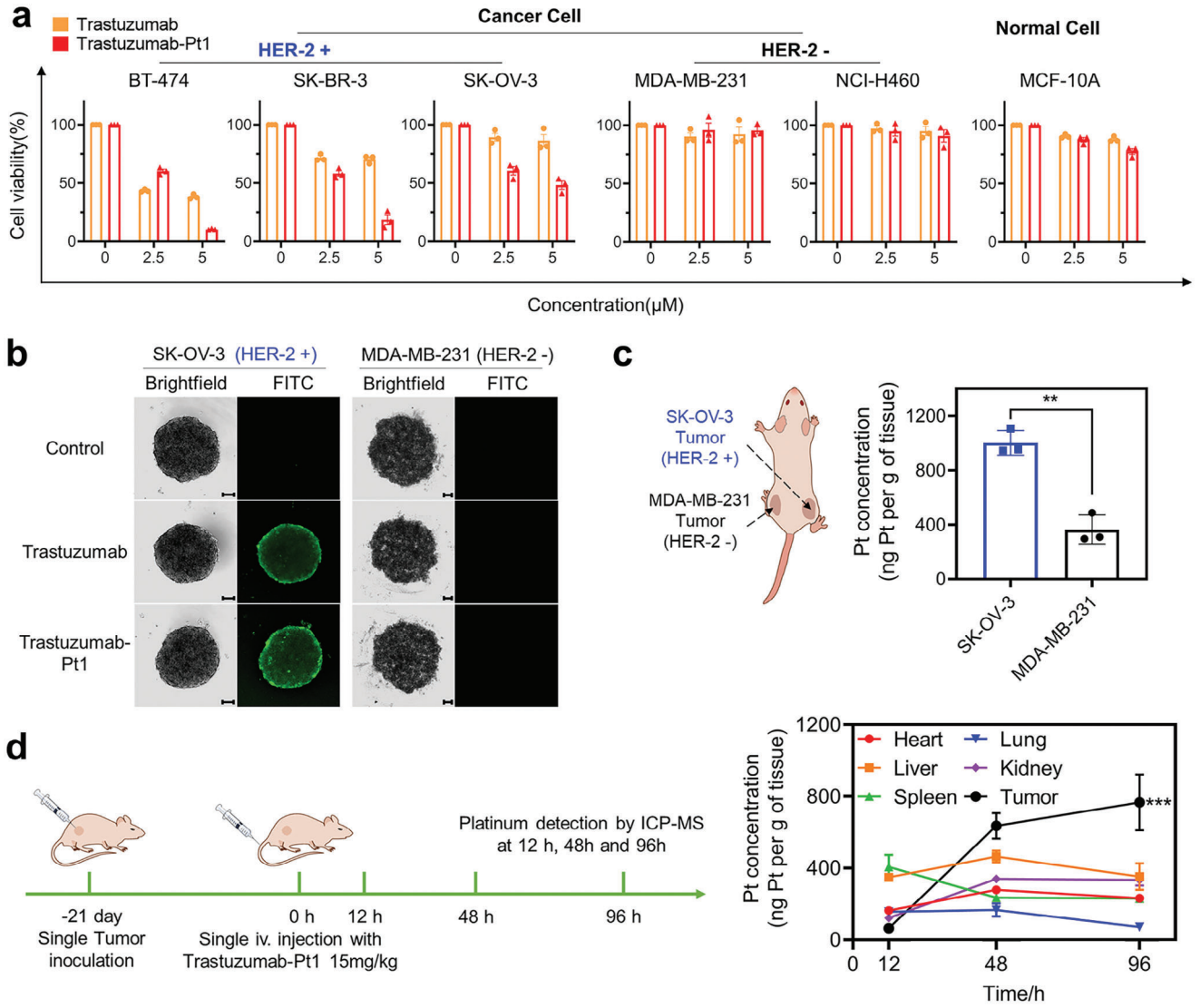

Figure 4. Targeting ability of **Trastuzumab-Pt1** in vitro and in vivo. a) The cytotoxicity of **Trastuzumab-Pt1** against different cell lines in vitro (Orange: trastuzumab, Red: **Trastuzumab-Pt1**). b) The ability of **Trastzumab-Pt1** to bind to HER-2 on the surface of 3D Tumor Spheroid (scale bar: 100 μm). c) The Pt concentration in different tumors of double tumor-bearing mice. ** means $p < 0.01$. d) The distribution of **Trastuzumab-Pt1** in vivo, as shown by a line graph. *** means $p < 0.001$.

During the 28-day observation period, tumor volume and body weight were measured every 2 days (**Figure** 5a). As shown in Figure 5b, on the 28th day of treatment, the 15 mg kg^{-1} **Trastuzumab-Pt1** group showed significant tumor inhibition, with a tumor volume of 166.3 ± 55.3 mm^3, which was only 1.7-fold higher than the original tumor volume (day 0). Meanwhile, the **Trastuzumab-Pt1** 10 mg kg^{-1} group showed a 2.6-fold increase (277.2 ± 121.8 mm^3). In comparison, the "Control" and "Trastuzumab" groups experienced substantial increases of 11.2-fold and 5.6-fold, reaching volumes of 1125.6 ± 173.5 mm^3 and 562.0 ± 90.5 mm^3, respectively. Additionally, tumors from each group were collected and weighed at the end of the study. The **Trastuzumab-Pt1** group achieved 75.9% (10 mg kg^{-1}) and 86.5% (15 mg kg^{-1}) tumor inhibition, which were higher the trastuzumab group (57.7%) and the control group (Figure 5d,e). In addition, we conducted in vivo comparisons between **Trastuzumab-Pt1** and **Pt-1**. The results demonstrated that **Trastuzumab-Pt1** exhibited superior anti-tumor efficacy, achieving a tumor inhibition rate of 65.3%. This was notably higher than that of an equal amount of **Pt-1** (19.4%) and even surpassed the group treated with a ten-fold higher dosage of **Pt-1** (50.0%) (Figure S18, Supporting Information).

It's worth noting that the Pt composition of the conjugate in the 15 mg kg^{-1} **Trastuzumab-Pt1** treatment group was only 0.051 and 0.034 mg kg^{-1} in the 10 mg kg^{-1} group (Table S4, Supporting Information). For this reason alone, the body weight of mice increased steadily during the 28-day study period (Figure 5c). In addition, no obvious damage or obvious inflammation-related lesions occurred in major organs including the lung, kidney, liver, spleen, and heart (Figure 5f). In comparison, the number of cells

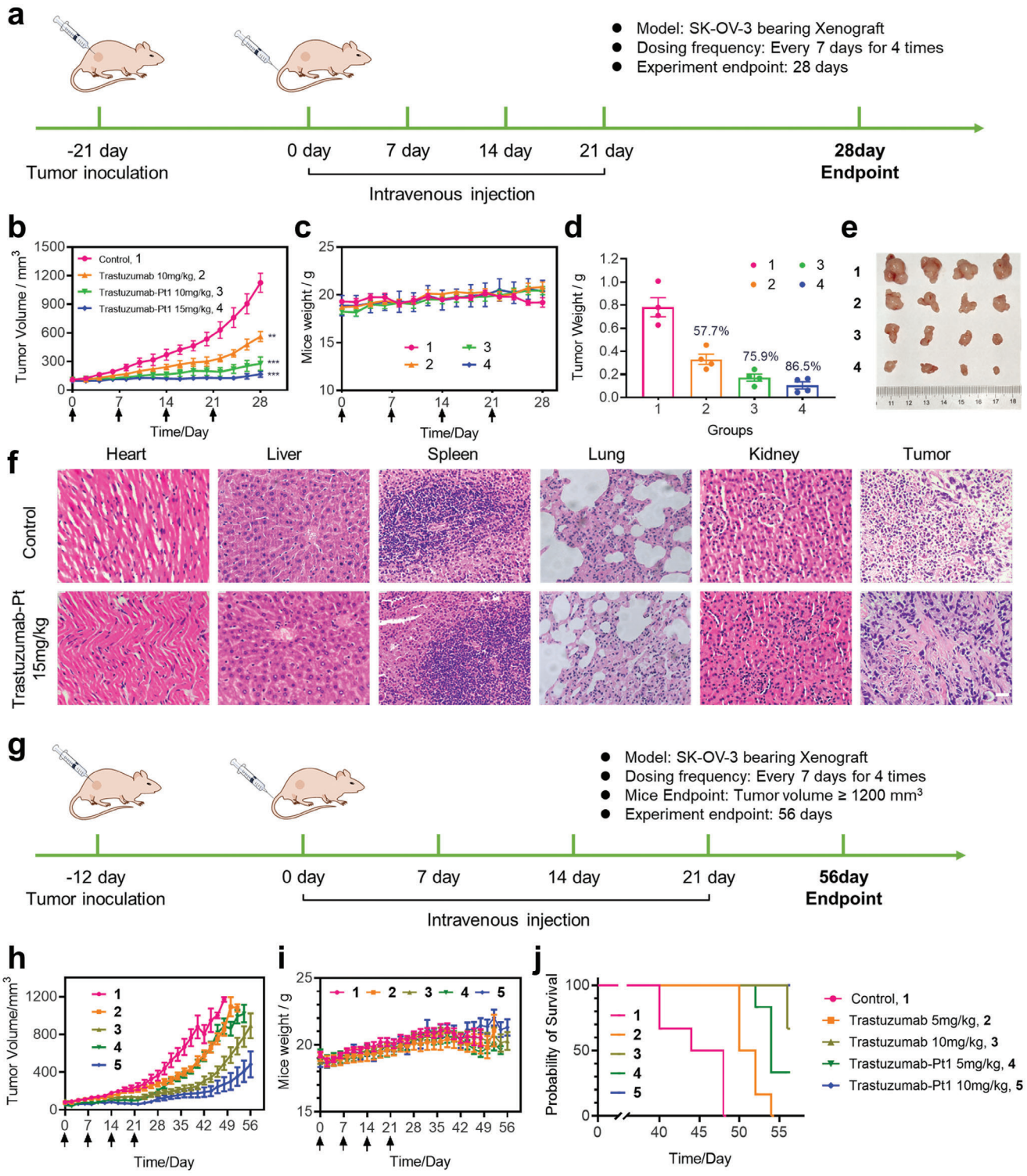

Figure 5. Anti-tumor efficacy of **Trastuzumab-Pt1** on SK-OV-3 xenograft tumor in nude mice. a) The scheme of a 28-day short-term SK-OV-3 xenograft tumor model. b) The tumor growth curves in different groups in the short-term model. Compare with control group, * means $p < 0.05$; ** $p < 0.01$; *** $p < 0.001$. c) The body weights of mice during the treatment in the short-term model. d) The final tumor weights after various treatments in the short-term model. e) The images of the tumor tissues in the short-term model. f) Hematoxylin and eosin (H&E) images of mice major tissues subject to different treatments. g) The scheme of a 56-day long-term SK-OV-3 xenograft tumor model. h) The tumor growth curves in different groups in the long-term model. i) The body weights of mice during the treatment in the long-term model. j) The survivorship curves of each group mice in the long-term model. There were no unplanned deaths, and all mice were mercifully executed when they reached the experimental endpoint (tumor volume ≈ 1200 mm^3 or 56 days). **Note**: The curve is not shown when there are fewer than three mice left in any group.

in tumors treated with **Trastuzumab-Pt1** was significantly decreased.

To evaluate the therapeutic effect of **Trastuzumab-Pt1** at the same dose as trastuzumab and tumor development at the end of administration, we established the SK-OV-3 xenograft model. In this model, 12 days after tumor inoculation, when the tumor volume was ≈50 mm^3, mice were randomly divided into five groups ($n = 6$), including "Control" group, "Trastuzumab 5 or 10 mg kg^{-1}" groups and the "**Trastuzumab-Pt1** 5 or 10 mg kg^{-1}" groups (Figure 5g). During the 56-day long-term observation period, tumor volumes and body weights were measured every 2 days, and mice were sacrificed once the tumor volume reached the predetermined experimental endpoint. On day 40 of treatment, the two tumors in the "Control" group reached 1200 mm^3, while the group that received the lower dose of **Trastuzumab-Pt1** (10 mg kg^{-1}) continued to show significant therapeutic effects, maintaining a tumor volume of 176.5 ± 100.5 mm^3. No significant toxicity (i.e., body weight loss of >20% or mice death) was induced in any group by the end of the study (Figure 5i). More importantly, as shown in Figure 5j, compared with "Control" ($P = 0.001$) and "Trastuzumab 10 mg kg^{-1}" ($P = 0.0209$), **Trastuzumab-Pt1** (10 mg kg^{-1}) provides improved survival benefit. None of their tumor volumes reached the experimental endpoint until day 56, even though two mice had tumor volumes (2/6) below 300 mm^3. This result highlights the advantage of conjugating metal complex **Pt-1** to trastuzumab to have good antitumor therapeutic effect in the treatment of ovarian tumors with small metal doses.

3. Conclusion

We synthesized a variety of pincer platinum(II) complexes using [CˆNˆN] ligands and *N*-heterocyclic carbene ligands containing hydroxyl or amino groups. These complexes can act on mitochondria, cause mitochondrial damage, and exhibit strong anti-tumor activity in vitro and in vivo. By conjugating the platinum(II) complex with trastuzumab to create novel platinum(II)-based antibody conjugate against HER-2, targeting selectivity and anti-tumor efficacy can be improved. We anticipate that more platinum(II)-based antibody conjugates will be developed and will be able to more effectively assist cancer patients in clinical settings.

4. Experimental Section

Details of the materials, experimental procedures, and data, including compound synthesis and characterization, photophysical measurements, X-ray crystallography, antibody-drug conjugation, in vitro anticancer, and in vivo antitumor assays are described in the Supporting Information.

Supporting Information

Supporting Information is available from the Wiley Online Library or from the author.

Acknowledgements

T.H. and W.-Q.H. contributed equally to this work. This work was supported by the Guangdong Basic and Applied Basic Research Foundation (2019B030302009, 2023A1515011759, 2023A1515030234, 2023A1515220204). The authors also acknowledge the funding support from "Laboratory for Synthetic Chemistry and Chemical Biology" under the Health@InnoHK Program launched by the Innovation and Technology Commission, The Government of Hong Kong Special Administrative Region of the People's Republic of China. Key (Guangdong-Hong Kong Joint) Laboratory for Preparation and Application of Ordered Structural Materials of Guangdong Province (2023B1212120011).

Conflict of Interest

The authors declare no conflict of interest.

Data Availability Statement

The data that support the findings of this study are available in the supplementary material of this article.

Keywords

antibody-drug conjugate, HER-2 targeted, immunogenic cell death, necroptosis, Pt(II) NHC

Received: September 11, 2024
Revised: January 28, 2025
Published online: February 14, 2025

[1] a) S. M. Sancho-Martinez, L. Prieto-Garcia, M. Prieto, J. M. Lopez-Novoa, F. J. Lopez-Hernandez, *Pharmacol. Ther.* **2012**, *136*, 35; b) B. W. Harper, A. M. Krause-Heuer, M. P. Grant, M. Manohar, K. B. Garbutcheon-Singh, J. R. Aldrich-Wright, *Chem. Eur. J.* **2010**, *16*, 7064; c) T. C. Johnstone, K. Suntharalingam, S. J. Lippard, *Chem. Rev.* **2016**, *116*, 3436.

[2] a) A. Brozovic, A. Ambriović-Ristov, M. Osmak, *Crit. Rev. Toxicol.* **2010**, *40*, 347; b) C. P. Tan, Y. Y. Lu, L. N. Ji, Z. W. Mao, *Metallomics* **2014**, *6*, 978.

[3] a) R. W.-Y. Sun, A. L.-F. Chow, X.-H. Li, J. J. Yan, S. S.-Y. Chui, C.-M. Che, *Chem. Sci.* **2011**, *2*, 728; b) T. Zou, C.-N. Lok, Y. M. E. Fung, C.-M. Che, *Chem. Commun. (Camb.)* **2013**, *49*, 5423; c) C. N. Lok, T. Zou, J. J. Zhang, I. W. Lin, C. M. Che, *Adv. Mater.* **2014**, *26*, 5550; d) S. K. Fung, T. Zou, B. Cao, T. Chen, W. P. To, C. Yang, C. N. Lok, C. M. Che, *Nat. Commun.* **2016**, *7*, 10655; e) T. T. Fong, C. N. Lok, C. Y. Chung, Y. M. Fung, P. K. Chow, P. K. Wan, C. M. Che, *Angew. Chem., Int. Ed.* **2016**, *55*, 11935; f) D. Hu, C. Yang, C. N. Lok, F. Xing, P. Y. Lee, Y. M. E. Fung, H. Jiang, C. M. Che, *Angew. Chem., Int. Ed.* **2019**, *58*, 10914; g) P. K. Wan, K. C. Tong, C. N. Lok, C. Zhang, X. Y. Chang, K. H. Sze, A. S. T. Wong, C. M. Che, *Proc. Natl. Acad. Sci. USA* **2021**, *118*, e2025806118.

[4] a) S. Y. Lin, S. Y. Hsieh, Y. T. Fan, W. C. Wei, P. W. Hsiao, D. H. Tsai, T. S. Wu, N. S. Yang, *Autophagy* **2018**, *14*, 778; b) K. Peng, Y. Zheng, W. Xia, Z. W. Mao, *Chem. Soc. Rev.* **2023**, *52*, 2790.

[5] a) O. Kepp, L. Galluzzi, M. Lipinski, J. Yuan, G. Kroemer, *Nat. Rev. Drug Discovery* **2011**, *10*, 221; b) L. Galluzzi, *Cell Death Differ.* **2018**, *25*, 486.

[6] Q. Zhang, L. Fan, G. Kuang, Y. Zhao, *Med. Plus* **2024**, *1*, 100002.

[7] a) S. Sen, M. Won, M. S. Levine, Y. Noh, A. C. Sedgwick, J. S. Kim, J. L. Sessler, J. F. Arambula, *Chem. Soc. Rev.* **2022**, *51*, 1212; b) L. Zhang, N. Montesdeoca, J. Karges, H. Xiao, *Angew. Chem., Int. Ed.* **2023**, *62*, e202300662; c) Z. Y. Li, Q. H. Shen, Z. W. Mao, C. P. Tan, *Chem. Asian J.* **2022**, *17*, e202200270; d) Z. Deng, H. Li, S. Chen, N. Wang, G. Liu,

D. Liu, W. Ou, F. Xu, X. Wang, D. Lei, P. C. Lo, Y. Y. Li, J. Lu, M. Yang, M. L. He, G. Zhu, *Nat. Chem.* **2023**, *15*, 930; e) Y. Huang, D. Wei, B. Wang, D. Tang, A. Cheng, S. Xiao, Y. Yu, W. Huang, *Acta Biomater.* **2023**, *160*, 198; f) X. Chang, M. Bian, L. Liu, J. Yang, Z. Yang, Z. Wang, Y. Lu, W. Liu, *Pharmacol. Res.* **2023**, *187*, 106556.

[8] F. Shi, X. Huang, Z. Hong, N. Lu, X. Huang, L. Liu, T. Liang, X. Bai, *Cancer Lett* **2023**, *562*, 216167.

[9] a) L. Galluzzi, A. Buque, O. Kepp, L. Zitvogel, G. Kroemer, *Cancer Cell* **2015**, *28*, 690; b) P. D. O'Dowd, D. F. Sutcliffe, D. M. Griffith, *Coord. Chem. Rev.* **2023**, *497*, 215439

[10] D. Y. Wong, W. W. Ong, W. H. Ang, *Angew. Chem., Int. Ed.* **2015**, *54*, 6483.

[11] R. Sharma, V. J. Singh, P. A. Chawla, *Anticancer Agents Med. Chem.* **2022**, *22*, 694.

[12] R. L. Lucaciu, A. C. Hangan, B. Sevastre, L. S. Oprean, *Molecules* **2022**, *27*, 6485.

[13] a) P. R. Hamann, L. M. Hinman, I. Hollander, C. F. Beyer, D. Lindh, R. Holcomb, W. Hallett, H. R. Tsou, J. Upeslacis, D. Shochat, A. Mountain, D. A. Flowers, I. Bernstein, *Bioconjug. Chem.* **2002**, *13*, 47; b) K. Tsuchikama, Y. Anami, S. Y. Y. Ha, C. M. Yamazaki, *Nat. Rev. Clin. Oncol.* **2024**, *21*, 203.

[14] a) N. Joubert, A. Beck, C. Dumontet, C. Denevault-Sabourin, *Pharmaceuticals (Basel)* **2020**, *13*, 245; b) R. V. Chari, M. L. Miller, W. C. Widdison, *Angew. Chem., Int. Ed.* **2014**, *53*, 3796; c) L. Zhou, Y. Lu, W. Liu, S. Wang, L. Wang, P. Zheng, G. Zi, H. Liu, W. Liu, S. Wei, *Exp. Hematol. Oncol.* **2024**, *13*, 26; d) F. van Delft, J. M. Lambert, *Chemical Linkers in Antibody–Drug Conjugates (ADCs)*, The Royal Society of Chemistry, CPI Group (UK) Ltd, Croydon, UK, **2021**.

[15] a) U. Hafeez, S. Parakh, H. K. Gan, A. M. Scott, *Molecules* **2020**, *25*, 4764; b) P. Khongorzul, C. J. Ling, F. U. Khan, A. U. Ihsan, J. Zhang, *Mol. Cancer Res.* **2020**, *18*, 3; c) P. S. S. Cindy H Chau, W. D. Figg, *Lancet* **2019**, *394*, 793.

[16] a) V. Del Solar, M. Contel, *J. Inorg. Biochem.* **2019**, *199*, 110780; b) C. Y. Lin, S. J. Yang, C. L. Peng, M. J. Shieh, *ACS Appl. Mater. Interfaces* **2018**, *10*, 6096.

[17] a) E. Hurwitz, R. Kashi, M. Wilchek, *J. Natl. Cancer Inst.* **1982**, *69*, 47; b) B. Schechter, R. Pauzner, R. Arnon, J. Haimovich, M. Wilchek, *Cancer Immunol. Immunother.* **1987**, *25*, 225; c) D. P. McIntosh, R. J. Cooke, A. J. McLachlan, P. T. DaleyYates, M. Rowland, *J. Pharm. Sci.* **1997**, *86*, 1478; d) R. Huang, Y. Sun, X.-y. Zhang, B.-w. Sun, Q.-c. Wang, J. Zhu, *Biomed. Pharmacother.* **2015**, *73*, 116; e) M. J. Matos, C. Labao-Almeida, C. Sayers, O. Dada, M. Tacke, G. J. L. Bernardes, *Chem. Eur. J.* **2018**, *24*, 12250; f) N. Curado, G. Dewaele-Le Roi, S. Poty, J. S. Lewis, M. Contel, *Chem. Commun. (Camb.)* **2019**, *55*, 1394; g) Z. Zhao, X. Tao, Y. Xie, Q. Lai, W. Lin, K. Lu, J. Wang, W. Xia, Z. W. Mao, *Angew. Chem., Int. Ed.* **2022**, *61*, e202202855; h) M. G. Rosenblum, J. L. Murray, S. Stuckey, R. A. Newman, S. Chaney, A. R. Khokhar, *Cancer Chemother. Pharmacol.* **1990**, *25*, 405; i) L. Ducry, B. Stump, *Bioconjug. Chem.* **2010**, *21*, 5.

[18] X. Wang, Z. Guo, *Chem. Soc. Rev.* **2013**, *42*, 202.

[19] a) K. Li, T. Zou, Y. Chen, X. Guan, C.-M. Che, *Chem. - Eur. J.* **2015**, *21*, 7441; b) K.-C. Tong, D. Hu, P.-K. Wan, C.-N. Lok, C.-M. Che, *Adv. Inorg. Chem.* **2020**, *75*, 87.

[20] L. Milane, M. Trivedi, A. Singh, M. Talekar, M. Amiji, *J. Controlled Release* **2015**, *207*, 40.

[21] W. Xu, J. Trepel, L. Neckers, *Cancer Cell* **2011**, *20*, 281.

[22] a) R. Brandt, A. S. Keston, *Anal. Biochem.* **1965**, *11*, 6; b) R. Cathcart, E. Schwiers, B. N. Ames, *Anal. Biochem.* **1983**, *134*, 111; c) W. Jakubowski, G. Bartosz, *Cell Biol. Int.* **2000**, *24*, 757; d) A. Cossarizza, R. Ferraresi, L. Troiano, E. Roat, L. Gibellini, L. Bertoncelli, M. Nasi, M. Pinti, *Nat. Protoc.* **2009**, *4*, 1790.

[23] J. Tornin, C. Labay, F. Tampieri, M. P. Ginebra, C. Canal, *Nat. Protoc.* **2021**, *16*, 2826.

[24] X. Xiong, Y. Wang, T. Zou, *ChemBioChem* **2023**, *24*, 202200621.

[25] K. Hanggi, B. Ruffell, *Trends Cancer* **2023**, *9*, 381.

[26] a) D. Tang, R. Kang, T. V. Berghe, P. Vandenabeele, G. Kroemer, *Cell Res.* **2019**, *29*, 347; b) A. G. Snyder, N. W. Hubbard, M. N. Messmer, S. B. Kofman, C. E. Hagan, S. L. Orozco, K. Chiang, B. P. Daniels, D. Baker, A. Oberst, *Sci. Immunol.* **2019**, *4*, eaaw2004.

[27] a) Z. Liu, X. Xu, K. Liu, J. Zhang, D. Ding, R. Fu, *Adv. Sci. (Weinh.)* **2023**, *10*, e2207475; b) G. Kroemer, C. Galassi, L. Zitvogel, L. Galluzzi, *Nat. Immunol.* **2022**, *23*, 487.

[28] a) Y. Anami, C. M. Yamazaki, W. Xiong, X. Gui, N. Zhang, Z. An, K. Tsuchikama, *Nat. Commun.* **2018**, *9*, 2512; b) Y. B. Poudel, C. Rao, S. Kotapati, M. Deshpande, L. Thevanayagam, C. Pan, J. Cardarelli, N. Chowdari, M. Kaspady, R. Samikannu, P. Kuppusamy, P. Saravanakumar, P. N. Arunachalam, S. Deshpande, V. Rangan, R. Rampulla, A. Mathur, G. D. Vite, S. Gangwar, *Bioorg. Med. Chem. Lett.* **2020**, *30*, 126782; c) C. M. Yamazaki, A. Yamaguchi, Y. Anami, W. Xiong, Y. Otani, J. Lee, N. T. Ueno, N. Zhang, Z. An, K. Tsuchikama, *Nat. Commun.* **2021**, *12*, 3528.

[29] a) V. Turk, B. Turk, D. Turk, *EMBO J.* **2001**, *20*, 4629; b) K. Hochdorffer, K. Abu Ajaj, C. Schafer-Obodozie, F. Kratz, *J. Med. Chem.* **2012**, *55*, 7502; c) N. G. Caculitan, J. D. Cruz Chuh, Y. Ma, D. Zhang, K. R. Kozak, Y. Liu, T. H. Pillow, J. Sadowsky, T. K. Cheung, Q. Phung, B. Haley, B. C. Lee, R. W. Akita, M. X. Sliwkowski, A. G. Polson, *Cancer Res.* **2017**, *77*, 7027.

[30] a) C. Villarroya-Beltri, F. Baixauli, M. Mittelbrunn, I. Fernandez-Delgado, D. Torralba, O. Moreno-Gonzalo, S. Baldanta, C. Enrich, S. Guerra, F. Sanchez-Madrid, *Nat. Commun.* **2016**, *7*, 13588; b) L. Opalinski, J. Szymczyk, M. Szczepara, M. Kucinska, D. Krowarsch, M. Zakrzewska, J. Otlewski, *Int. J. Mol. Sci.* **2018**, *19*, 1435; c) Y. Wang, S. Fan, D. Xiao, F. Xie, W. Li, W. Zhong, X. Zhou, *Cancers (Basel)* **2019**, *11*, 957; d) M. Y. Chin, A. R. Patwardhan, K. H. Ang, A. L. Wang, C. Alquezar, M. Welch, P. T. Nguyen, M. Grabe, A. V. Molofsky, M. R. Arkin, A. W. Kao, *ACS Sens.* **2021**, *6*, 2168.

[31] a) J. Harper, S. Mao, P. Strout, A. Kamal, *Methods Mol. Biol.* **2013**, *1045*, 41; b) Y. Yao, L. Yu, X. Su, Y. Wang, W. Li, Y. Wu, X. Cheng, H. Zhang, X. Wei, H. Chen, R. Zhang, L. Gou, X. Chen, Y. Xie, B. Zhang, Y. Zhang, J. Yang, Y. Wei, *J. Controlled Release* **2015**, *220*, 5; c) J. C. Kang, W. Sun, P. Khare, M. Karimi, X. Wang, Y. Shen, R. J. Ober, E. S. Ward, *Nat. Biotechnol.* **2019**, *37*, 523; d) H. F. Zong, X. Li, L. Han, L. Wang, J. J. Liu, Y. L. Yue, J. Chen, Y. Ke, H. Jiang, Y. Q. Xie, B. H. Zhang, J. W. Zhu, *Acta Pharmacol. Sin.* **2024**, *45*, 1727.